Process diagnostics and thickness metrology using *in situ* mass spectrometry for the chemical vapor deposition of W from H_2/WF_6

Theodosia Gougousi, Yiheng Xu, John N. Kidder, Jr., and Gary W. Rubloff[a)]
Institute for Systems Research and Department of Materials and Nuclear Engineering, University of Maryland, College Park, Maryland 20742

Charles R. Tilford
National Institute of Standards and Technology, Process Measurement Division, Gaithersburg, Maryland 20899

(Received 14 December 1999; accepted 3 March 2000)

Quadrupole mass spectrometry has been used to monitor reactant and product partial pressures in a selective W chemical vapor deposition process. A $4/1 H_2/WF_6$ molar reactant ratio was used to produce W films on Si wafers, at 67 Pa (0.5 Torr) total pressure, and for wafer temperatures around 400 °C. A relatively fast response time (~4 s) sensor system sampled gas directly from a commercial Ulvac ERA-1000 reactor in order to minimize the effect of wall reactions. The signal from the volatile HF product, integrated over the deposition cycle, and corrected for contributions from reactions in the ion-source region of the quadrupole and for sensor drifts, was found to vary linearly with the weight of the W film deposited, to within an uncertainty of ~7%. This provides the basis for real-time, noninvasive thickness metrology to drive process control. Depletion of both H_2 and WF_6 reactants was observed. The time integral of the H_2 reactant depletion was also linearly related to the film weight, though the data exhibited a somewhat larger scatter due to the low conversion efficiency of the process. In addition, volatile SiF_4 and $SiHF_3$ products of the initial rapid W nucleation reaction on the Si surface were clearly observed, indicating that initial surface conditions may be monitored in real time under selective growth conditions. © *2000 American Vacuum Society.* [S0734-211X(00)08103-8]

I. INTRODUCTION

The manufacturing of integrated circuits involves deposition or growth of material layers whose thickness and properties must conform to very strict standards. In most cases, the success of the process is determined by post-process analysis of product or monitor wafers, delaying the time at which process errors are detected. This can lead to major yield losses before problems are discovered and corrected. As a result, real-time process monitoring for metrology, process control, and fault management promises major benefit in process productivity and cost.[1]

An ideal real-time chemical sensor for monitoring processes involving multicomponent gas mixtures would provide information on reactants, products, and contaminants. Due to its versatility, mass spectrometry is one of the primary candidates. It has been used for considerable time in manufacturing environments to detect basic contaminants and more recently, in successful application for fault detection in industrial environments.[2] However, for quantitative analysis and wafer state metrology, the linearity and stability of mass spectrometer sensors are concerns, particularly, when they are implemented *in situ* and exposed to reactive process environments. Nevertheless, properly configured mass spectrometers have been successfully used for measuring deposition rates and establishing thickness metrology during poly-Si[3,4] and gate oxide rapid-thermal chemical vapor deposition (RTCVD).[5] They have also been effectively employed to monitor plasma etching[6] and deposition processes.[7,8]

Optical techniques also provide chemical sensitivity but with a different set of concerns. Laser spectroscopy methods and Fourier transform infrared spectroscopy (FTIR) provide broad chemical selectivity but are species specific and involve complex instrumentation with a substantially lower experience base in manufacturing environments. Optical emission spectroscopy (OES) has been widely used as a process endpoint monitor in plasma etching, but its nonlinearity, associated with the plasma, is an obstacle to quantification, while the requirement for optically excited state species limits its applications to plasma processes alone. Laser interferometry has become routine for etch endpointing, and its full-wafer imaging embodiment (full-wafer interferometry)[9] represents the first serious *in situ* measure of across-wafer process uniformity, but it has so far been restricted to plasma etching processes.

Thus, quantitative chemical sensing for process metrology remains a substantial research challange critical to advanced process control. In this article, we present results demonstrating that mass spectrometers can be used for predicting the W film weight (thickness) resulting from H_2 reduction of WF_6 with an accuracy better than 10%. This provides promise for an *in situ,* real-time thickness metrology sufficient to support robust process control strategies.[10]

[a)]Author to whom correspondence should be addressed; electronic mail: rubloff@isr.umd.edu

II. W CVD PROCESS

Deposition of W films on Si surfaces (or, to be precise, on a seed W layer) can be achieved through the reduction of WF_6 or either H_2 or SiH_4.[11] In the first pathway, used in the current work, the Si surface provides the initial nucleation layer for the formation of a seed W layer

$$3Si+2WF_6 \rightarrow 2W(s)+3SiF_4\uparrow, \quad (1)$$

$$3Si+WF_6 \rightarrow W(s)+3SiF_2\uparrow, \quad (2)$$

and

$$2Si+WF_6+H_2 \rightarrow W(s)+2SiHF_3\uparrow. \quad (3)$$

Once this W seed layer achieves complete coverage of the wafer surface, it provides the active sites for the H_2 reduction of the WF_6 through adsorption and F-atom removal from the surface as the volatile HF product

$$W^{\star}(s)+WF_6 \rightarrow WF_6^{\star}+W(s), \quad (4)$$

$$WF_6^{\star}+3H_2 \rightarrow W(s)^{\star}+6HF\uparrow, \quad (5)$$

where * denotes an activated surface site. For each W atom deposited on the surface, three molecules of H_2 and one molecule of WF_6 are consumed, and six molecules of HF are produced. Monitoring of the time evolution of the gas phase reactant H_2 and product HF with a quadrupole mass spectrometer provides the basis for a film thickness metrology.

Tungsten (W) deposition is of major industrial interest and application, with blanket CVD in broad use for contact hole filling involving significant conformality requirements associated with the increasing aspect ratio of contact structures. Our work has used a lower pressure version (67 Pa or 0.5 Torr) of the blanket H_2/WF_6 CVD process (which is typically operated at ~5 kPa or 40 Torr), because the Ulvac tool was designed for a lower-pressure selective W deposition process. This lower-pressure version of the blanket process is relatively inefficient, with a low utilization efficiency for the process gases, and correspondingly smaller process signals. It is, in many ways, a worst-case test of our process sensing technique.

III. EXPERIMENT

A. Reactor design and normal process cycle

The W CVD process was carried out using an Ulvac ERA-1000 cluster tool, which has been described in detail in another publication.[12] In brief, the tool consisted of two single wafer reactors, along with a buffer and a load-lock chamber for automated loading and transfer of wafers as large as 200 mm (8 in.). Each reactor was water cooled to prevent deposition on the walls and equipped with two sets of pumps: (1) Roots blower and heavy-duty mechanical pump for maintaining gas flow while processing, and (2) mechanically backed turbopump for maintaining reactor cleanliness while idling. The reactor pressure was measured either by ion gauge or capacitance diaphragm gauge depending on the operation status (idle versus process), while the reagent supply was regulated by mass flow controllers. The H_2 reagent was supplied through a perforated quartz showerhead on the top of the reactor above the wafer surface, while the WF_6 reagent was admitted through a slit on the side at the wafer level. During deposition, the wafer was placed on a rotating susceptor to ensure azimuthal symmetry of the film. Halogen lamps situated outside and above the reactor provided heating to the wafer through a quartz window. An integrated controller received status signals from several sensors in the cluster tool and controlled the sequence of operations and the process parameters (pressure, temperature, reactant flow rates, and duration of each process step), preset by programmable process recipes. The tool capabilities allowed sequential processing of up to 15 wafers, thus minimizing the idle time between depositions.

In the Ulvac, nominal wafer temperature is controlled by lamp power in combination with a thermocouple located outside the reactor. To test the temperature accuracy, an instrumented wafer with five thermocouple sensors was used in the presence of H_2 and N_2 reagents to compare actual wafer temperature to the nominal control temperature on the tool. The actual temperature of the wafer was found significantly lower (~100 °C) than the nominal temperature presented by the tool control system. Furthermore, the instrumented wafer measurements revealed that the wafer temperature was not stable through the process cycle. Instead, wafer heating approached a steady value over minutes and depended critically on the heating protocol. Therefore, we implemented a modification to the heating cycle, which delivered considerably higher power to the heating lamps in the initial portion of the cycle. This provided a reasonably constant (~5%) temperature profile through the deposition cycle, with very small radial nonuniformity (less than 2%). For experiments performed at a programmed temperature of 500 °C, the real wafer temperature was closer to 400 °C. This correction brought the observed deposition rates and conversion rates into consistency with those expected from established process models[11] and our own simulations.[13]

B. Wafer preparation and process

All the experiments presented in this article were performed on 100 mm (4 in.) Si wafers which had undergone cleaning in 10% HF solution, de-ionized (DI) water rinsing, and N_2 drying. The H_2 and WF_6 reagents (research grade) were used without any further purification. An optimal process window was identified at a total pressure of 67 Pa (0.5 Torr), actual wafer temperature around 400 °C, and with reagent flows of 40 sccm (standard cubic centimeters of gas/min) for H_2 and 10 sccm for WF_6.

C. Sampling system location and wall reactions

The initial location for the quadrupole mass spectrometer (QMS) sampling system was chosen to be just before the process pumps, which are located several meters downstream from the reactor, in the chase or support area just outside the clean room wall. The choice was intended to minimize interference with the tool (i.e., not to restrict either tool operation

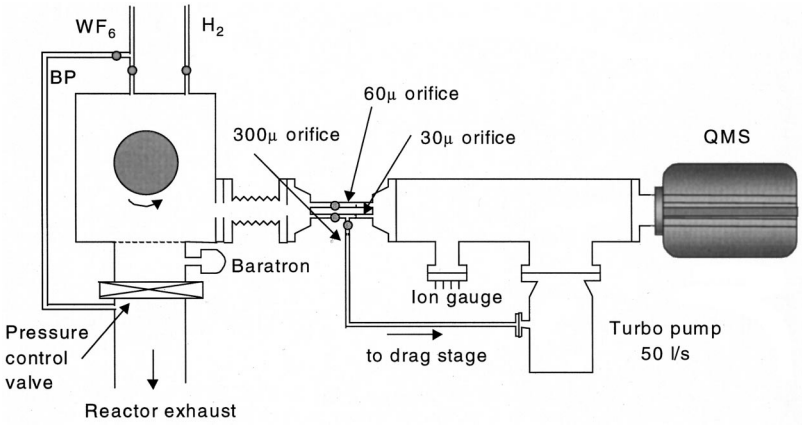

FIG. 1. Schematic diagram of the CVD reactor and the mass spectrometer sampling system. The drag stage of the turbodrag pump is used to draw process gas downstream of the wafer and a 30 μm orifice allows the introduction of a portion of the gas into the closed ion source of the mass spectrometer for analysis. The 60 μm orifice was not used in the course of this work.

or maintenance) and to preserve floor space inside the clean room. Previous experience with rapid thermal SiH_4-based CVD processes for poly-Si[3,4] and oxide[5] deposition provided promising real-time thickness metrology data using this downstream sampling location, and the aim of this work was to extend the approach to the W CVD process. The chemistry in the previous two cases was quite favorable, due to the relative inertness of SiH_4 with respect to interactions at chamber walls and in exhaust pump lines at room temperature. However, the high reactivity of both reactants and products in the W CVD case has prevented us from obtaining with this configuration sufficiently reproducible data to establish a thickness metrology.

Both the WF_6 reactant and the HF product condense readily on all available surfaces at room temperature, and the large area of the exhaust line provided a very efficient condensation surface, introducing memory effects, so that even hours of operation were not sufficient to stabilize the wall conditions. Furthermore, the efficiency of the process in our tool was quite low (2%–3% reactant conversion), reducing the available signals associated with product generation and reactant depletion, while important ion-molecule reactions in the sensor ion source produced large amounts of background HF. As a result, the downstream sampling method was abandoned, and the new sensing system was implemented to sample gas directly at the reactor.

D. Mass spectrometry sampling system

The new configuration (Fig. 1) reduces significantly the wall area between the process and the sensor. A separate inlet to the drag step of the turbodrag pump (Pfeiffer) on the mass spectrometer system was used to draw a small amount of the process gas downstream of the heated wafer through a 300 μm orifice in the gas sampling system (Leybold–Inficon) (Fig. 1). A 30 μm orifice allowed the introduction of a fraction of that gas into the turbopumped quadrupole mass spectrometer chamber for mass analysis. A 300 amu closed-ion source Leybold–Inficon instrument operated in the Faraday Cup ion collection mode was used for data collection. Typically, for process pressure of 67 Pa (0.5 Torr), the pressure in the quadrupole region of the mass spectrometer was 5×10^{-4} Pa (4×10^{-6} Torr). The sampling configuration exhibited a response time of 3–4 s to process gas composition changes in the reactor. While this can be improved, it was quite sufficient for this application, where the usual deposition time was 6 min.

E. Impurity control

The new sensing system, including both gas-sampling lines and mass spectrometer, is temperature controlled at 70 °C to minimize the wall adsorption of reactants/products and gas phase impurities such as H_2O. Control of impurity species, particularly H_2O, is very important in all vacuum applications, but even more so in the case of WF_6 processes: H_2O readily reacts in the gas phase with WF_6 even at room temperature, producing HF product[14] by the reaction

$$2WF_6+4H_2O\rightarrow WOF_4\uparrow+WO_3+8HF\uparrow \quad (6)$$

and thus providing another extraneous and uncontrollable sourced of the main species used for metrology.

Several steps were taken to reduce these impurity problems in addition to temperature control. Before data were taken, the reactor/sampling system was conditioned with the reactant gas mixture until the walls reached equilibrium and the impurities were minimized, which took anywhere from a few minutes to several hours depending on the system's history. The criterion for completing this conditioning procedure was the relative intensity of WF_5^+ and WOF_3^+, which are the main species resulting from the fragmentation of the WF_6 and WOF_4 in the ion source. Experience demonstrated that a WF_5^+ to WOF_3^+ ratio of about 4 was sufficiently low for good quality sensing data. Total elimination of the WOF_4 impurity is impossible in systems, such as ours, which incorporate stainless steel surfaces, since WF_6 reacts with the oxidized surface of stainless steel to generate WOF_4 and other species.[15]

F. Sensor integration

A LabView™-based software platform was used for data collection. Signals from the mass spectrometer as well as from the tool controller (reactor pressure, wafer nominal temperature, mass flow controller set points, and valve sta-

tus) were collected simultaneously. This allowed direct, time-synchronized correlation between the chemical sensing data and the process state signals.

In the initial stages of the work, mass spectra throughout the 300 amu range were collected with an unheated wafer (no deposition) to record the cracking patterns of the reagents. This was repeated during deposition until all the relevant reaction products were identified. When all the species of interest were selected, then the random scan capability of the software was utilized to record time profiles of selected mass peaks through the process cycle. In this mode, the mass spectrometer samples only the selected peaks (up to 10), thus allowing a much faster data collection rate (0.5 s per data point increment).

G. Process conditions

The ULVAC ERA-1000 tool is designed for a selective deposition process involving SiH_4 reduction of WF_6, which normally takes place at pressures below 133 Pa (1 Torr) and temperatures around 350–400 °C. In contrast, blanket W CVD processes using H_2 reduction of WF_6, which now dominate the industry, typically operate at slightly higher temperatures and considerably higher pressures (5 kPa). Our experiments attempted to exploit the Ulvac reactor for the H_2 reduction process, but were limited to lower pressures than those normally employed for the blanket process. Initial experiments at 27 Pa (0.2 Torr) and nominal 500 °C temperature with 10/1 H_2 to WF_6 reactant ratio indicated surprisingly poor conversion rates (of the order of 1%) compared to our expectations from known deposition rates and process models.

Attempts to raise the temperature further, or to increase the pressure above 67 Pa (0.5 Torr), resulted in loss of deposition selectivity, causing deposition of W on the reactor walls and on the quartzware surrounding the wafer. For the selective deposition process, further deposition could then occur where selectivity loss had previously led to W deposition, particularly on the quartzware. As a result, the effective deposition area (intended to be the wafer surface area) would increase in a history-dependent fashion, making it impossible to correlate the sensor signals from different runs.

In industrial practice, the H_2/WF_6 reactant ratio is typically of order 4 or less in order to obtain sufficiently high conformality for via filling. Process analyses indicate that low H_2/WF_6 ratios cause rate limitations associated with H_2 transport, and that the chemistry of H_2 reaction on the growth surface exploits a lower sticking probability to achieve high conformality.[11] As a result, we used a H_2/WF_6 reactant ratio of 4 in much of this work. We used a dynamic equipment and process simulator[12,13] to investigate how process parameters influence detectability in chemical sensing. This revealed that the lower flow rates, at the same pressures and reactant stoichiometries, could significantly improve sensitivity. Some of the initial experiments were conducted at a nominal temperature of 500 °C and 67 Pa (0.5 Torr), with 200 sccm of H_2 and 50 sccm of WF_6 (H_2/WF_6 ratio of 4). When both of the reactant flow rates were reduced by a factor of 5 (to 40 sccm of H_2 and 10 sccm of WF_6) at the same temperature and pressure settings, reactant conversion was significantly enhanced. The HF product signal increased from only 5% to about 25% above the background HF produced in the ion source. Thus, process parameters were maintained to 40 sccm of H_2 and 10 sccm of WF_6, 67 Pa (0.5 Torr), and nominal temperature of 500 °C (actual wafer temperature about 400 °C). This change also increased the H_2 conversion rate to ~2%–3%, making the depletion observable in the mass spectrometry data.

H. Process cycle for chemical sensing and metrology

During the course of the peak identification routine, it was found that a significant amount of HF was produced by gas phase reactions in the ion source of the sensor and by wall reactions. To obtain an accurate baseline measurement for this important metrology species, the process recipes were modified to include a ''cold'' wafer step. Thus, the following operation sequence was followed: (a) The wafer was loaded and H_2 flow was introduced to purge the reactor. (b) The reagent mixture (H_2/WF_6) was flowed at the process pressure over a ''cold'' (room temperature) wafer (denoted as the ''cold wafer'' step) to obtain an accurate baseline for all interesting species. (c) The WF_6 was diverted to a reactor bypass line, and the wafer was heated to the deposition temperature in the presence of H_2 only. (d) With the heating lamps on to maintain the wafer ''hot'' (denoted as the ''hot wafer'' step), the WF_6 was redirected back to the chamber and the deposition began; and (e) the WF_6 flow and the wafer heating were terminated, and a large flow of H_2 was used to cool down the wafer prior to removal.

IV. RESULTS

A. Mass spectrometry sampling through the process cycle

A typical set of ion current data obtained from the quadrupole mass spectrometer (QMS) includes time stamped information for up to ten peaks of interest. Figure 2 shows the temporal evolution of several signals for species of interest in the process, such as the reactants H_2 and WF_6 represented by H_2^+ (2 amu) and WF_5^+ (279 amu) respectively, the products HF, SiF_4, and $SiHF_3$ represented by HF^+ (20 amu), SiF_3^+ (85 amu), and $SiHF_2^+$ (67 amu) and the major impurity species H_2O and WOF_4 represented by H_2O^+ (18 amu) and WOF_3^+ (257 amu). For the WF_6 and WOF_4, the ^{184}W isotope peak was chosen. Figure 2 illustrates a complete process cycle including both the ''cold wafer'' and ''hot wafer'' steps described earlier. Particularly noteworthy is the high HF signal evident during the ''cold wafer'' step, which is the result of ion-molecule reactions initiated by the presence of the reactants in the sensor ion source. Nevertheless, the difference in the HF levels between the ''cold wafer'' and the ''hot wafer'' steps is quite evident, this difference reflecting the additional HF product generation associated with W deposition in the reactor. The selectivity of the process should also be noted; the onset of the deposition process is

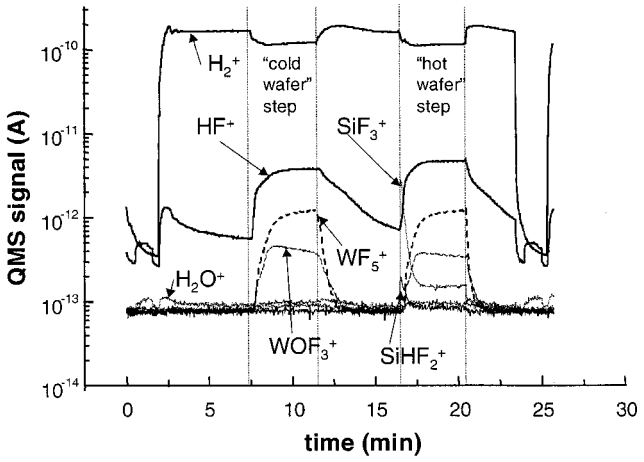

FIG. 2. A typical set of data collected during a film deposition run. The monitored species include the reactants H_2 and WF_6, the main reaction product HF, the nucleation step products SiF_4 and $SiHF_3$, and H_2O and WOF_4 impurities. Noteworthy is the high HF background seen in the ''cold wafer'' step, which is produced from gas phase reactions occurring in the sensor. Nevertheless, the difference in the HF levels between the ''cold wafer'' and the ''hot wafer'' steps is quite evident. The intensity of the SiF_4 signal (seen here as SiF_3^+), is about 20× that of $SiHF_3$ (appearing as $SiHF_2^+$), indicating that nucleation reaction (1) is the major channel for the production of the seed W layer.

marked by the appearance of the SiF_4 and $SiHF_3$ species resulting from the self-limiting W nucleation reactions (1) and (3) on the hot Si wafer surface.

The level of H_2O impurities is quite low, about 30% higher than the noise level associated with the ion currents captured in the Faraday cup. The major source of H_2O was chamber contamination introduced from the load-lock during the wafer transfer (note the H_2O peak at the beginning of the cycle). Following the wafer transfer to the reactor, the chamber was flushed with H_2 for about 5 min to remove these contaminants. The level of the WOF_4 impurity in these data is 3.5× lower than the WF_5^+ level, close to the best ratios we have achieved.

The notable reduction in the H_2 levels between steps 1 and 2 in Fig. 4 is mainly due to the changing gas composition in the reactor. During the first step, only H_2 (40 sccm) was present at a total pressure of 67 Pa (0.5 Torr), while during the second step, WF_6 (10 sccm) was added. Since the total reactor pressure was kept constant at 67 Pa (0.5 Torr), the corresponding H_2 partial pressure changed to 53 Pa (0.4 Torr). However, the change in the mass spectrometer signals is somewhat larger than the proportional change in H_2 partial pressure. This is attributed to reactions (mainly ion-molecule) in the ion source that deplete some of the reagents, typical of the kinds of complexity involved in chemical sensing for this reactive system. In this system, such reactions lead to the formation of HF, which is observed during the ''cold wafer'' (unheated wafer) step as a significant background HF concentration.

B. Mass spectrometry analysis for thickness metrology

Figures 3 and 4 show examples of the HF and H_2 signals respectively for a single run with the steps of the process cycle in time identified. The ''cold wafer'' step and ''hot wafer'' step are marked with open circles to focus attention on the portions of the process cycle which are crucial to metrology. The ''cold wafer'' portion exhibits background signals existing in the absence of deposition on the wafer, since the wafer is at room temperature, while the ''hot wafer'' step includes both these background signals and that from deposition on the wafer. The HF signal (Fig. 3) exhibits a significant (~25%) increase from ''cold wafer'' to ''hot wafer'' conditions, reflecting evolution of the reaction product associated with deposition in the reactor. The H_2 signal shows a smaller (~2%) but discernible decrease in going from ''cold wafer'' to ''hot wafer,'' attributed to depletion of the H_2 reactant during the deposition reaction.

A better illustration of the HF production and the H_2 depletion is provided by overlaying the ''cold wafer'' and the ''hot wafer'' portions of the signal, as provided by the small inserts in the upper right hand corner of Figs. 3 and 4, respectively. The areas of the shaded regions in the inserts represent the amount of HF generation and H_2 depletion associated with the deposition reaction. Since the effect of the reaction is clearly larger, under the conditions studied, for the HF product generation, HF is expected to provide the better metrology signal. In the course of this work, we used both signals and achieved consistent results from the two signals, as shown below, but the larger HF signal provided a more precise basis for metrology.

C. Run-to-run reproducibility and drift

A successful metrology requires that the process signals are reproducible over a number of runs. Figures 5(a) and 5(b) show HF and H_2 signals for a batch of six wafers processed for different deposition times but otherwise under identical conditions. The signals are well behaved and fairly reproducible. The combined drift of the sensor and the process is of the order of 5% during the 4 h that this multiwafer experiment lasted, which is typical of all data sets collected. Although not very large, this 5% drift can introduce a significant uncertainty in the metrology data. Introduction of the ''cold wafer'' step in the process serves to eliminate this additional source of error. To illustrate better the magnitude of the wafer-to-wafer signal drift the ''cold wafer'' data for these six runs are overlaid in Fig. 6. The small difference in the signal amplitude between the various runs indicates sensor and/or process drifts.

It should be pointed out that the small ripples in the HF signal in Fig. 6, as well as in the H_2 signal during the beginning of the cycle in Fig. 4, are real effects. They are associated with small oscillations in the reactor pressure caused by the pressure control system, and are particularly notable in Fig. 4 where the reactor must be quickly filled with H_2, and the control system shows overshoot and damped oscillation.

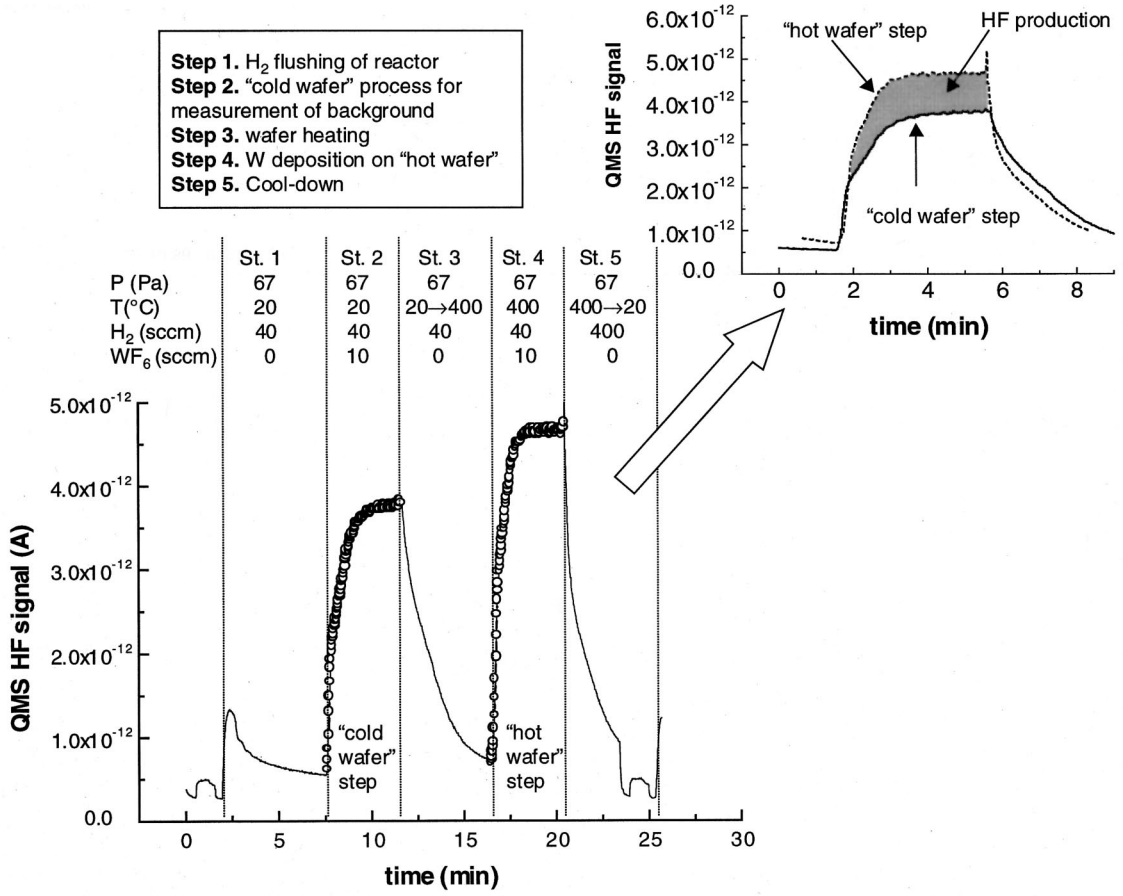

FIG. 3. Temporal evolution of the HF signal for a 4 min deposition cycle (large graph). The portion of the graph with the open circles indicates the process steps of importance (''cold wafer'' and ''hot wafer'' steps with both H_2 and WF_6 reagents flowing through the reactor). The small graph above and to the right shows an overlay of the two steps mentioned before, to illustrate better the HF production during the W deposition step. Details of the process parameters are given in the table above the large figure (for the ''hot wafer'' step a best estimate for the real wafer temperature is given).

D. Thickness metrology from mass spectrometry

To establish a thickness metrology, the HF and H_2 signals, corrected for background and sensor drifts, must be related to the total W film weight or thickness as measured postprocess. Mathematical manipulation of the data consisted of five steps for both HF product generation and H_2 depletion. (1) The signals during the ''cold wafer'' and ''hot wafer'' steps were each integrated over the duration of the step and corrected for the residual HF [see Figs. 5(a) and 6] to obtain integrated areas A_{CW} and A_{HW}. (2) The ratio $D(H_2)$ of the A_{HW} to the A_{CW} area for H_2 was calculated to provide the average unreacted portion of the H_2 reagent during the process. Due to the reagent depletion, the ''cold wafer'' HF area $[A_{CW}(HF)]$ is an upper limit (assuming no deposition) for the HF background. Experimental data suggested that for our process conditions, the HF background area was the first approximation proportional to the H_2 concentration: a 2% utilization of the H_2 (typical for our process) during the process should result to an equal reduction in the $A_{CW}(HF)$. (3) The differences between A_{CW} and A_{HW} for H_2 (or between A_{HW} and $D(H_2)^{\star}A_{CW}$ for HF) were computed to provide a measure of the changes associated with the reaction. (4) The differences were normalized to the ''cold wafer'' area A_{CW} for H_2 or $D(H_2)^{\star}A_{CW}$ for HF. (5) These results were then multiplied by the deposition times T (i.e., the duration of the ''cold wafer'' or ''hot wafer'' steps) to achieve mass-spectrometry-derived thickness metrology signals.

Thus, for HF product generation, the metrology signal is given by

$$S_{HF}=\frac{A_{HW}(HF)-D(H_2)A_{CW}(HF)}{D(H_2)A_{CW}(HF)}\,T,$$

where

$$D(H_2)=\frac{A_{HW}(H_2)}{A_{CW}(H_2)}$$

corresponding to the increase in HF signal from ''cold wafer'' to ''hot wafer'' step associated with product generation. For H_2 depletion, the metrology signal is given by

$$S_{H_2}=\frac{A_{CW}(H_2)-A_{HW}(H_2)}{A_{CW}(H_2)}\,T$$

corresponding to the decrease in H_2 signal from ''cold wafer'' to ''hot wafer'' step associated with depletion of the H_2

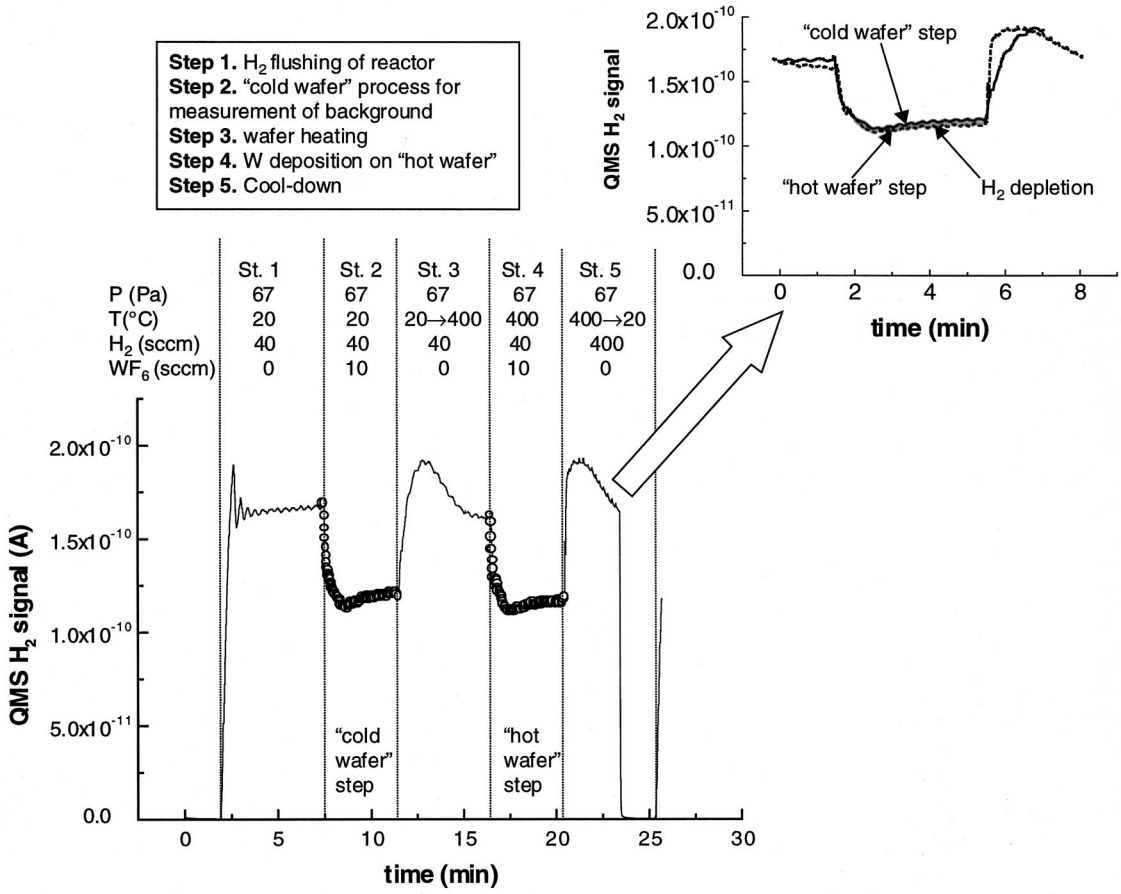

FIG. 4. Temporal evolution of the H_2 signal for a 4 min deposition cycle (large graph). The portion of the graph with the open circles indicates the process steps of importance (''cold wafer'' and ''hot wafer'' steps with both H_2 and WF_6 reagents flowing through the reactor). The small graph above and to the right shows an overlay of the two steps mentioned before, to illustrate better the H_2 reactant depletion during the W deposition step. Details of the process parameters are given in the table above the large figure (for the ''hot wafer'' step a best estimate for the real wafer temperature is given).

reactant. This somewhat lengthy mathematical manipulation was found necessary for correction of the errors resulting from the sensor/process drifts and the depletion of the reagents.

The W film weight was determined by measuring the wafer weight before and after the deposition with a microbalance. To prevent errors due to drifts in the microbalance, the weight of a test wafer was recorded prior to each set of measurements and used for mass scale calibration. Errors in the microbalance measurement were found small compared to those resulting from noise in the mass spectrometry metrology signals. The microbalance provided a much faster and more accurate assessment of deposition amount compared to lithographic patterning and profilometry. Once the film weight is known, the average thickness is easily calculated from the known wafer area and W density.[16] While this could mask thickness nonuniformities across the wafer, the mass spectrometer signal for metrology is also insensitive to across-wafer nonuniformities.

Figures 7 and 8 illustrate the relationship between the W film weight and the HF and H_2 normalized mass spectrometer signals, respectively. The relationship is fairly linear in both cases, with the HF data giving better results as a result of the larger signal associated with the deposition reaction. Accordingly, a regression analysis was carried out to reveal the best linear fit to the data (with one clearly extraneous data point in Fig. 8 omitted).[17]

In the case of HF product sensing, the regression analysis generates the expression (shown by the straight line):

$$\text{Film weight (g)} = 0.0080(\pm 0.0003) S_{\text{HF}} + 0.0047(\pm 0.0006).$$

In the case of H_2 reactant depletion sensing, the model expression (shown by the straight line) is

$$\text{Film weight (g)} = 0.0888(\pm 0.0065) S_{\text{H}_2} + 0.0063(\pm 0.0012).$$

The S factors are those described above for calculating reaction-associated signals from the data. Uncertainties are one standard deviation.

E. Nucleation on the Si surface

Note that there is a positive y intercept in the graphs in Figs. 7 and 8, i.e., some W is deposited before either HF product or H_2 depletion is observed. This is associated with the nucleation reaction, which initially deposits a seed layer

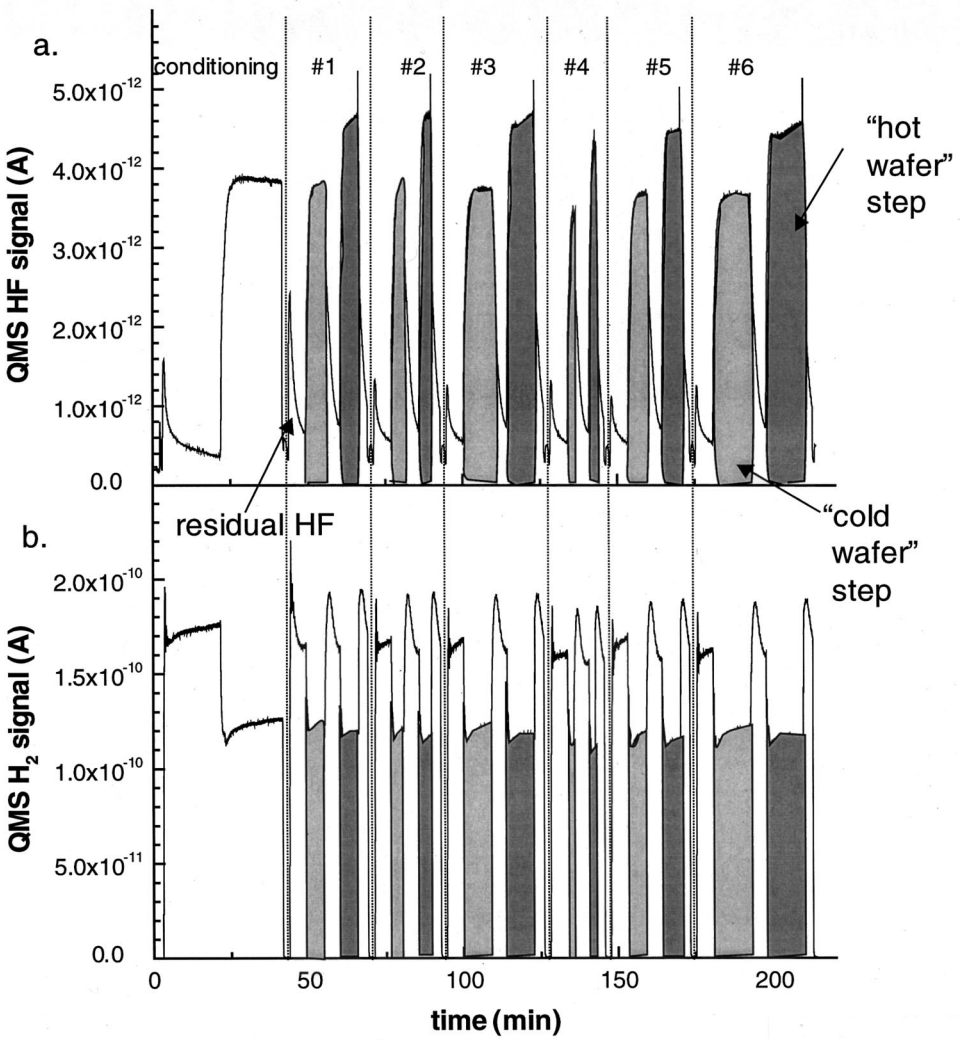

FIG. 5. Time evolution of the HF (a) and the H_2 (b) signals for a 6 wafer deposition run. Before the deposition is begun, a 40 min conditioning cycle is executed to equilibrate the sensor and sampling system walls. For each deposition cycle, initially a ''cold wafer'' step is executed to provide a baseline signal with which the actual deposition (''hot wafer'' step) signals will be compared. Both signals are well behaved and the monotonic sensor drift is of the order of 5% in the course of the experiment.

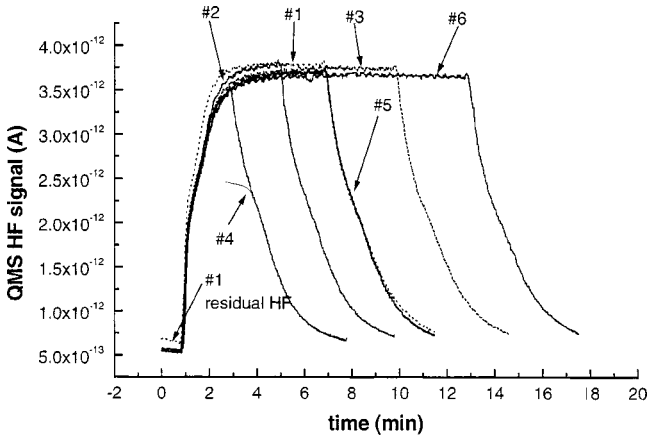

FIG. 6. Overlay of the HF signals for the ''cold wafer'' step spectra from the experiment shown in Fig. 5(a). Initially there is a small reduction in the amplitude of the signal with wafer number (analogous to a ''first wafer'' effect), but for the last three runs, the HF signals are reproducible to about 1%. Note the higher HF signal on the onset of the first wafer's ''cold wafer'' step.

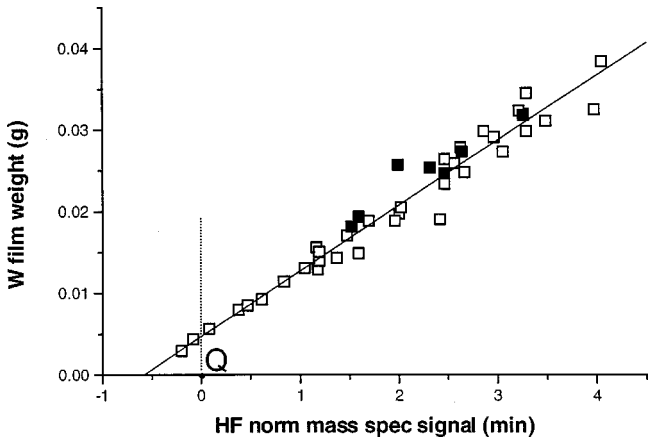

FIG. 7. W film weight vs the HF signal (normalized HF production above background times deposition time). The solid points indicate the ''first'' wafer in each experimental run. The solid line is a linear regression through all data points. Point *Q* denotes the beginning (0,0) of the axes.

of W on the bare Si surface by the Si reduction reactions (1) to (3) given above. Evidence for this nucleation step is found in the mass spectrometry signals in Fig. 2: at the start of the ''hot wafer'' step of the process, where deposition occurs, sharp spikes of SiF_3^+ (indicative of SiF_4 product) and of $SiHF_2^+$ (indicative of $SiHF_3$ product) are seen. These are the expected products generated by the nucleation reactions given in (1) and (3). Thus, the initial W seed layer is deposited on the Si surface without generating either HF product of H_2 depletion, leading to the positive *y* intercept in Figs. 7 and 8.

To verify this, the H_2 reagent was replaced by Ar and with no further change in the process conditions a few of the deposition runs were repeated. In the absence of H_2, only reactions (1) and (2) may occur, and the weight of the W seed layer was found 0.0040 ± 0.0003 g, which is within the two-sigma uncertainties of the values obtained from both the HF and H_2 data. The weight of this self-limiting W layer resulting from the WF_6 reduction in the Ar atmosphere corresponds to a film thickness of 26 nm [16] in excellent agreement with measurements performed by Melliar-Smith *et al.*[18] and Yu and Eldridge.[19] This shows that the nucleation reaction channel (1), i.e., $3Si+2WF_6 \rightarrow 2W(s)+3SiF_4\uparrow$, is the dominant channel even in the presence of H_2. In turn, this may explain why so little HF evolution is observed through the H_2 reduction reaction during the initial deposition phase.

In fact, the first two points of Fig. 7 indicate a negative HF production (i.e., HF depletion). These two data points correspond to very short deposition times (15 and 30 s, respectively), during which the nucleation reactions dominate in the process. HF depletion during the nucleation phase is consistent with the mass spectrometry data, as shown in Fig. 9. The HF signal for the ''cold wafer'' condition (no reaction on the wafer) rises more rapidly with time than does the signal for the ''hot wafer'' condition (reaction on the wafer), producing an area (shown in Fig. 9 as ''initial HF depletion'') in which the mass spectrometry HF signal decreases. We attribute this effect to ion source reactions: with significant WF_6 depletion in the nucleation step, less unreacted WF_6 reaches the sensor, and accordingly less background HF signal associated with H_2-WF_6 reactions in the ion source occur (the very reactions which intrinsically produce HF in the ''cold wafer'' step). Thus, the apparent negative HF production is really an artifact consisting of a change (reduction) in the HF background produced within the sensor.

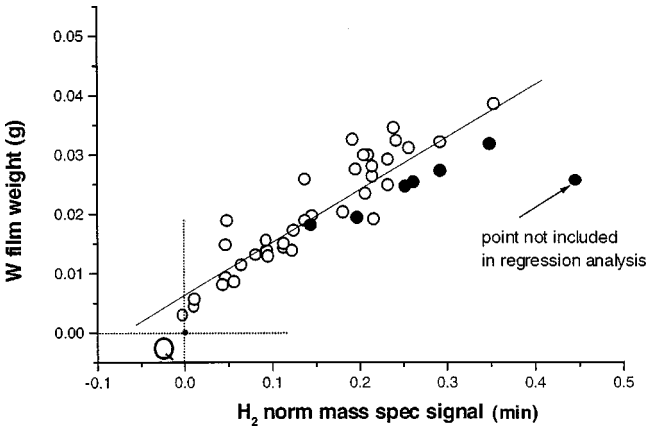

FIG. 8. W film weight vs the H_2 signal (normalized H_2 depletion times deposition time). The solid points indicate the ''first'' wafer in each experimental run. The solid line is a linear regression through all data points except from the point marked on the graph. No rational explanation can be provided for the large deviation of that specific point. Point *Q* denotes the beginning (0,0) of the axes.

V. DISCUSSION

A. Process chemistry

Real-time, *in situ* sensing of the gaseous species in the reactor through the process cycle provides information on the mechanisms of the specific reaction. The data illustrated here constitute experimental verification of the primary chemical mechanisms of the H_2 reduction reaction. In addition, the results indicate that for the H_2/WF_6 ratio of 4 used for these experiments, the nucleation reaction on the Si surface is dominated by the reaction $3Si+2WF_6 \rightarrow +2W(s)+3SiF_4\uparrow$ rather than by that involving hydrogen $2Si+WF_6+H_2 \rightarrow W(s)+2SiHF_3\uparrow$, since the SiF_4 product signal is $\sim 20\times$ stronger than that for $SiHF_3$. This conclusion is based on the assumption that the ionization efficiency and the mass

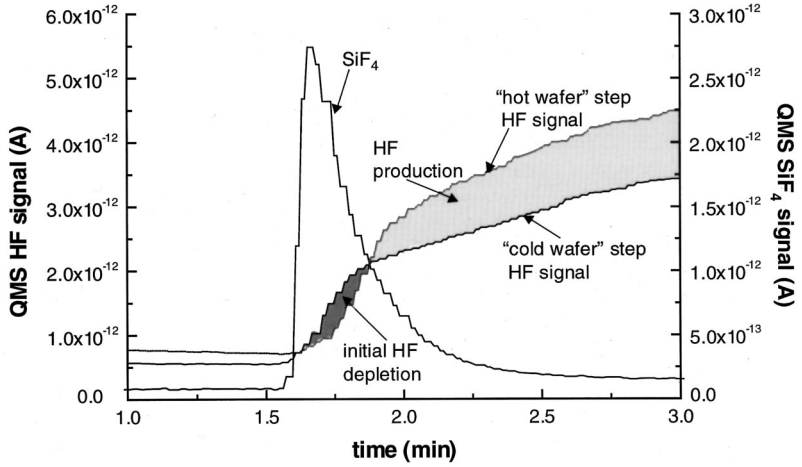

FIG. 9. Enlarged version of the small graph from Fig. 3. The SiF_4 is included so as to time stamp the beginning of the deposition. For the first 20–30 s of the deposition, the HF signal for the ''hot wafer'' step is smaller than the corresponding signal for the ''cold wafer'' step. This is attributed to the role of the self-limiting nucleation reaction in depleting WF_6, thus leading to smaller production of HF in the sensor ion source. When the nucleation reaction is completed, then the HF production for the ''hot wafer'' step exceeds that of the background ''cold wafer'' step.

filter transmission functions are quite similar for both species, which is reasonable since there is very small difference in their structure and mass.

Additional experiments indicated a variation in the relative significance of the two channels for different process conditions (H_2/WF_6 ratio, and process pressure). It must be noted here that traces of SiF^+ (comparable in magnitude to the $SiHF_2^+$) were also observed in the mass spectrum. Since this species can originate from the fragmentation of all Si containing products of the nucleation reactions (1)–(3), no quantification on the relative importance of reaction $3Si + 3WF_6 \rightarrow 3W(s) + 3SiF_2\uparrow$ could be made except to state that this reaction is probably the least important of the three under our conditions. Such an observation agrees with experimental data of Yu *et al.*[20] who found that for process temperatures below 400 °C, reaction (1) dominates the Si reduction of WF_6. By comparison, the high SiF_4 to SiF_2 ratio observed in our process provides confirmation that the real wafer temperature is close to 400 °C rather than the 500 °C value indicated by the tool controller.

B. ''First wafer effects'' in chemical sensing

Some of the points on both Figs. 7 and 8 are marked with a solid instead of an open symbol. These points represent the first wafer in each batch (total of 7 batches). For the HF based metrology, these points exhibit a systematic deviation from the linear regression fit: all the first wafer points lie to the ''left'' of the best fit, while for the H_2 data, the first wafer points all lie to the ''right'' of the regression line. Nevertheless, in both cases, the scattering is similar to the scattering for the rest of the points.

''First wafer effects'' are well known, particularly in plasma etching, from their effect on processes. However, this ''first wafer effect'' has a different origin and significance, associated with the history of gas flow conditioning in the reactor, amplified by the detailed complexities of reactions in the mass spectrometer ion source. The sensor mechanisms can be understood as follows. Each process cycle was started and finished with a H_2 flush of the reactor in order to remove (i) the impurities entering from the buffer chamber during wafer transfer and (ii) excess WF_6 from the surfaces. The excess WF_6 removal shows up as increased HF formed in the ion source. This effect can be observed in Fig. 5(a), where in the beginning of each cycle, a spike of HF is detected. The HF spike was larger for the first wafer, due to the absence of the final H_2 purge from the conditioning cycle. The 5 min H_2 purge in the beginning of the cycle was not sufficiently long to bring the level of the excess WF_6 down to the levels achieved during the rest of the cycles. Although an estimate (based on linear extrapolation) of this residual HF has been subtracted from all data, it is possible that the method led to slight overestimation of the ''cold wafer'' HF area A_{CW} for the first wafer, which may have resulted in underestimation of the process originated HF product.

However, a process related ''first wafer'' effect has been observed in the course of our work: in plots of the film weight as a function of the deposition time some of the ''first wafers'' seemed to deviate significantly (as much as 30%) from the general trend. While the origin of these process related ''first wafer'' effects are not yet fully understood, it is very encouraging that the sensor signals successfully detected these process deviations, as can be seen in Fig. 7. This provides an indication of the sensitivity and reliability of the technique. The origin of these process related ''first wafer'' effects has not been understood yet. Further investigation of such process-related ''first wafer effects,'' as well sensor-initiated ''first wafer effects'' will be undertaken in future research on run-to-run control in this system.

C. Statistical analysis

Although the uncertainties in the coefficients of the regression fits in Figs. 7 and 8 provide a general idea for the quality of the linear fit, a more rigorous error calculation is required so as to provide an estimate for the accuracy of the method. For that purpose, the residual for each data point was calculated, where the residual is defined as the difference between the actual y values for each data point and the values resulting from the linear regression fit. Then, the absolute value of the residual was divided by the regression-predicted value to obtain the fractional uncertainty. The average uncertainty thus calculated for the HF data was 6.5%, while for the H_2 data was 17%. The standard error of the predicted film weight for each x value (HF production or H_2 depletion) in the regression was found 0.0019 g for the HF data and 0.0039 g for the H_2 data. (The standard error is a measure of the error in the prediction of y value for an individual x.) For the case of HF sensing, the standard error is less than half of the weight of the nucleation layer and results in about an 8% uncertainty in the prediction of the film weight for a typical 6 min deposition process. Slight improvement in these uncertainties is obtained when the regression fit is done in the absence of the first wafer data.

D. Reactant conversion efficiency

An important checkpoint for the validity and applicability of the method is whether the QMS signals constitute an accurate representation of the process. For example, calculation of the conversion (depletion) rates for the H_2 reactant based on the amount of material that was deposited on the wafer are in very good agreement with the average depletion ($\sim$2.5%) indicated by the QMS. Clearly, such very low reagent conversion rate (2%–2.5% for H_2 and about 3% for WF_6) is very undesirable from the point of view of industrial process efficiency, as well as chemical sensing reliability.

E. Metrology signal choices

In addition to the H_2 depletion, the WF_5^+ signal (representing the WF_6) exhibits a marginal depletion between the ''cold wafer'' and the ''hot wafer'' steps. Because the WF_6 depletion signals are small, and because of wall reactions which lead to the formation of the WOF_4 impurity, they were judged inadequate for metrology.

In principle, both the HF product and the H_2 and WF_6 depletion signals could be candidates for thickness metrology sensing. The experience in this research suggests that the choice of a signal on which to base thickness metrology is dependent on the specific process. Here, the requirement of via filling and associated high conformality dictates a relatively low H_2/WF_6 ratio, which translates into similar conversion rates for both reagents. However, the far less problematic wall chemistry for H_2 makes the H_2 depletion-based metrology more favorable. The HF product signal, in fact, provides the most attractive signal, because its background, arising from reactions in the ion source, is less an impediment. However, the HF based metrology was achieved after extensive investigations on the effects of the wall conditioning and the process conditions in general.

F. Blanket W CVD process

The practical significance of this work was compromised by the current inability of the reactor to operate in the regime typically employed for blanket W CVD processes. One reactor of the Ulvac ERA-1000 tool is presently being converted to substrate heating for operation at higher pressures, including the blanket W CVD process operating at ~5 kPa (40 Torr). For manufacturing processes, reagent conversion rates around 50% are typically achieved. This is not only beneficial with regard to the costs of consumables in manufacturing, as well as environmental mass balance consequences, but it is also expected to enhance the sensitivity and accuracy of the mass spectrometer based metrology. With large reagent conversion rates, the H_2 signal is expected to provide the best signal for metrology purposes, almost free of the complications associated with sensor reactions that plague the HF based metrology. Under such conditions, the HF based metrology seems relatively less favorable since the ''cold wafer'' HF signal will have to be scaled to provide the appropriate background for the ''hot wafer'' step (due to the high depletion of the reagents). The favorable conclusions of the present work make the mass spectrometry approach to *in situ* thickness metrology promising, and deserving of further study.

G. Thickness metrology for run-to-run control

The objective of this research has been to develop a thickness metrology to support run-to-run control. Thickness measurements with an accuracy of 10% seem borderline to drive a control methodology, although even measurements with errors of this magnitude can, when combined with robust control algorithms, help to minimize run-to-run process drifts. However, for processes with realistic conversion rates for manufacturing (10–20× that obtained here), thickness metrology should be substantially better. Beyond this, keeping in mind that the low conversion efficiency of the present process greatly increases the process sensing problems, a number of factors will have to be considered in evaluating the potential benefits of mass-spectrometer-based thickness metrology in a realistic blanket W CVD process. These include a more complete characterization of process stability, sensor reproducibility and sensitivity, relative signal strengths for different process conditions, and the relative contributions of systematic versus random drifts in the process.

VI. CONCLUSIONS

A quadrupole mass spectrometer has been successfully used for chemical monitoring of a W CVD process. Time-integrated signals of the HF reaction product and the H_2 reactant were strongly correlated with the weight of the W film deposited. Of the two signals, the HF-based metrology achieved a greater sensitivity and provided a prediction of wafer thickness with an average uncertainty of ~6.5%. This is comparable to the precision achieved with SiH_4-based rapid thermal CVD of poly-Si,[3] despite the more challenging chemistry involved in the W CVD process, and the low conversion efficiency in comparison to that found for blanket W CVD processes in common industrial use. For industrial processes, it is expected that the H_2 signal will be more useful for metrology purposes.

This accomplishment required extensive experimental refinements and the development of a new sampling system for direct gas sampling from the reactor rather than the reactor exhaust as originally planned. Reagent adsorption on the walls, as well as wall reactions were especially challenging requiring attention to wall conditioning prior to deposition runs and temperature control of the sampling system. While this might appear to be a concern in a manufacturing application, such practices are already in use in industrial environments.[21]

Ion-molecule reactions in the mass spectrometer ion source also provided a significant source of HF background signals. This background and sensor/process drifts necessitated calibration measurements with a ''cold wafer'' step in the process, in which the reactants flowed through the reactor without wafer heating, so that the mass spectrometer could be properly calibrated and normalized against drifts associated with wall reactions and the sensor. Such additional process time per wafer would be a serious concern in manufacturing, but we have identified and are pursuing approaches for *in situ* partial-pressure calibration of the mass spectrometer. Preliminary experiments are promising and have demonstrated that this calibration can be performed without adversely affecting the process cycle time.

In the course of this work, we identified and quantified the nucleation reaction, which forms the initial seed layer of W on the Si surface. In the presence of both WF_6 and H_2, the formation of the W seed layer is dominated by the WF_6 reduction on the Si surface as indicated by the evolution of the SiF_4 product.

These results demonstrate that reasonable thickness metrology may be obtained using mass spectrometry in highly reactive CVD environments, including those where wall reactions are substantial. Of course, metrology in itself delivers value when coupled with a process control approach, which is the ultimate goal of our research. We believe that the impact of this work will be determined by two key factors.

First, as we adapt this methodology to blanket W processes typical of those in commercial use, conversion rates and mass spectrometry signals will increase, thereby improving the accuracy of the *in situ* metrology. The extent of this improvement is yet to be determined, but the current work encourages us to believe metrology signals with the accuracy and run-to-run reproducibilities demanded in manufacturing are achievable. Second, as we implement robust run-to-run[10] control algorithms, the benefit may be largely limited by the relative size of random vs systematic process drift. The motivation for adopting advanced process control methods is often to compensate for systematic drifts, and to the extent they dominate, the mass-spectrometry-based metrology reported here will be of substantial value.

ACKNOWLEDGMENTS

The authors are grateful to Dr. Louis Frees and Dr. Robert Ellefson of Leybold Inficon for close technical support, continuing cooperation, and for donation of the reactor sampling system. They are also indebted to Hsiao-Yung Chang for obtaining the instrumented wafer temperature data and to Laurent Henn-Lecordier for providing substantial technical assistance with the ULVAC tool. This work has been supported in part by Texas Instruments through the Semiconductor Research Corporation's Research Customization program, by the National Institute of Standards and Technology, and by the National Science Foundation. Specification of commercial products is for identification purposes only and does not imply endorsement by the National Institute of Standards and Technology.

[1]*National Technology Roadmap for Semiconductors 1997* (SIA Semiconductor Industry Association, San Jose, CA, www.semichips.org, 1998).
[2]J. M. Baker, Abstract in the 45th International Symposium of the American Vacuum Society, Baltimore, November 1998, p. 192.
[3]L. L. Tedder;, G. W. Rubloff, B. F. Conaghan, and G. N. Parsons, J. Vac. Sci. Technol. A **14**, 267 (1996).
[4]L. L. Tedder, G. W. Rubloff, I. Shareef, M. Anderle, D. H. Kim, and G. N. Parsons, J. Vac. Sci. Technol. B **13**, 1924 (1995).
[5]G. Lu, L. L. Tedder, and G. W. Rubloff, J. Vac. Sci. Technol. B **17**, 1417 (1999).
[6]X. Li, M. Schaepkens, G. Oehrlein, R. E. Ellefson, L. Frees, N. Mueller, and N. Korner, J. Vac. Sci. Technol. A **17**, 2438 (1999).
[7]A. I. Chowdhury, W. W. Read, G. N. Parsons, G. W. Rubloff, and L. L. Tedder, J. Vac. Sci. Technol. B **15**, 127 (1997).
[8]A. I. Chowdhury, T. M. Klein, T. M. Anderson, and G. N. Parsons, J. Vac. Sci. Technol. A **16**, 1852 (1998).
[9]K. Wong, D. S. Boning, H. H. Sawin, S. W. Butler, and E. M. Sachs, J. Vac. Sci. Technol. A **15**, 1403 (1997).
[10]S. Adivikolanu and E. Zafiriou, IEEE Trans. Compon., Packag. Manuf. Technol. Part A **23**, 56 (2000).
[11]J. J. Hsieh, J. Vac. Sci. Technol. A **11**, 3040 (1993).
[12]N. Gupta, Y. Xu, L. Henn-Lecordier, T. Gougousi, J. N. Kidder, Jr., and G. W. Rubloff (unpublished).
[13]Y. Xu, T. Gougousi, N. Gupta, J. N. Kidder, Jr., and G. W. Rubloff (unpublished).
[14]R. V. Joshi, V. Prasad, M. L. Yu, and G. Scilla, Appl. Phys. (N.Y.) **71**, 1428 (1992).
[15]D. A. Bell, Z. Lu, J. L. Falconer, and C. M. McConica, Conference Proceedings, VLSI VI, Materials Research Society, 1991, p. 31.
[16]For 10.16 cm (4 in.) wafers, a W film weighing 0.01 g has a thickness of 66 nm.
[17]One point in Fig. 8 deviates very strongly (by at least three standard deviations) from the general trend exhibited by the rest of the data. While the mathematical analysis of the data was checked and rechecked, no rational explanation for this point could be identified, and the data point has been omitted from the regression analysis as involving a substantial error of unknown origin.
[18]C. M. Melliar-Smith, A. C. Adams, R. H. Kaiser, and R. A. Kushner, J. Electrochem. Soc. **121**, 298 (1974).
[19]M. L. Yu and B. N. Eldridge, J. Vac. Sci. Technol. A **7**, 625 (1989).
[20]M. L. Yu, K. Y. Ann, and R. V. Joshi, IBM J. Res. Dev. **34**, 875 (1990).
[21]J. M. Baker (private communication).